CrossMark

Modeling environmental controls on the transport and fate of early life stages of Antarctic krill (*Euphausia superba*) on the western Antarctic Peninsula continental shelf

Andrea Piñones [a,c,*], Eileen E. Hofmann [a], Kendra L. Daly [b], Michael S. Dinniman [a], John M. Klinck [a]

[a] *Center for Coastal Physical Oceanography, Old Dominion University, 4111 Monarch Way, 3rd floor, Norfolk, VA 23508, USA*
[b] *College of Marine Science, University of South Florida, 140 Seventh Avenue South, St. Petersburg, FL 33701, USA*
[c] *Department of Geology and Geophysics, Yale University, P.O. Box 208109, New Haven, CT 06520-8109, USA*

A B S T R A C T

A one-dimensional, temperature-dependent model was used to simulate the descent–ascent cycle of the embryos and early larval stages of Antarctic krill to determine which regions of the western Antarctic Peninsula (wAP) continental shelf support successful completion of this cycle under present environmental conditions and those projected to occur as a result of climate change. The transport and fate of the embryo and larva under present and modified conditions was investigated with Lagrangian particle tracking simulations. The two modeling studies were implemented using temperature and density (embryo–larva model) and circulation distributions (Lagrangian particle tracking) obtained from a high resolution version of the Regional Ocean Modeling System configured for the wAP shelf region. Additional simulations used temperature and circulation distributions obtained from simulations that were forced with increased wind speed and increased transport of the Antarctic Circumpolar Current (ACC), both projected to possibly occur with climate change in the wAP region. Simulations using present conditions showed that successful completion of the descent–ascent cycle occurred along the outer shelf and on the shelf in regions with bottom depths of 600–700 m. Estimated residence times for the shelf regions that support success of the embryo and larva were 20–30 days. Thus, krill spawned in the mid and inner shelf regions can be retained in these regions through development to the first feeding stage (calyptopis 1). Increased winds and ACC transport resulted in more onshelf transport of Circumpolar Deep Water (CDW), which increased the volume of warm (1–1.5 °C) water at depth. These conditions supported a moderate increase in success of the krill embryo and larva, but only for limited areas of the shelf where hatching depths decreased by 10–30 m (< 5%) and development time to the calyptopis 1 stage decreased by 15–20%. The modified circulation conditions also supported increased advection of krill larvae into areas of the shelf that would experience the largest reduction of sea ice, especially in winter. Projected changes in wind strength and CDW transport may potentially enhance larval survival and advection onto the wAP shelf, but recruitment may be decreased by modifications to local sea ice distributions that would impede survival of Antarctic krill that overwinter on the shelf.

1. Introduction

The Antarctic krill (*Euphausia superba*) distribution along the western Antarctic Peninsula (wAP) continental shelf (Fig. 1) is maintained by local and remote inputs, as suggested by observational (Lascara et al., 1999; Fraser and Hofmann, 2003; Pakhomov et al., 2004; Wiebe et al., 2011) and modeling studies (Piñones et al., 2011, 2013). The contribution from local inputs on the wAP continental shelf depends on the abundance and location of spawning stock and the ability for the Antarctic krill embryo to hatch at a depth shallow enough for the larva to return to the sea surface (the descent–ascent cycle; Marr, 1962). The distribution of Antarctic krill spawning stock and spawning grounds on the wAP continental shelf was inferred from observations that showed spatial separation of the life stages and seasonally varying distributions in biomass (Siegel, 1988, 1992). Juveniles and early subadults were observed in the inner shelf region and gravid and spent females were found along the outer shelf and in oceanic

* Corresponding author at: Department of Geology and Geophysics, Yale University, P.O. Box 208109, New Haven, CT 06520-8109, USA.
Tel.: +1 203 432 7767; fax: +1 203 432 3134.
E-mail addresses: andrea.pinones@yale.edu,
mpinones@ccpo.odu.edu (A. Piñones).
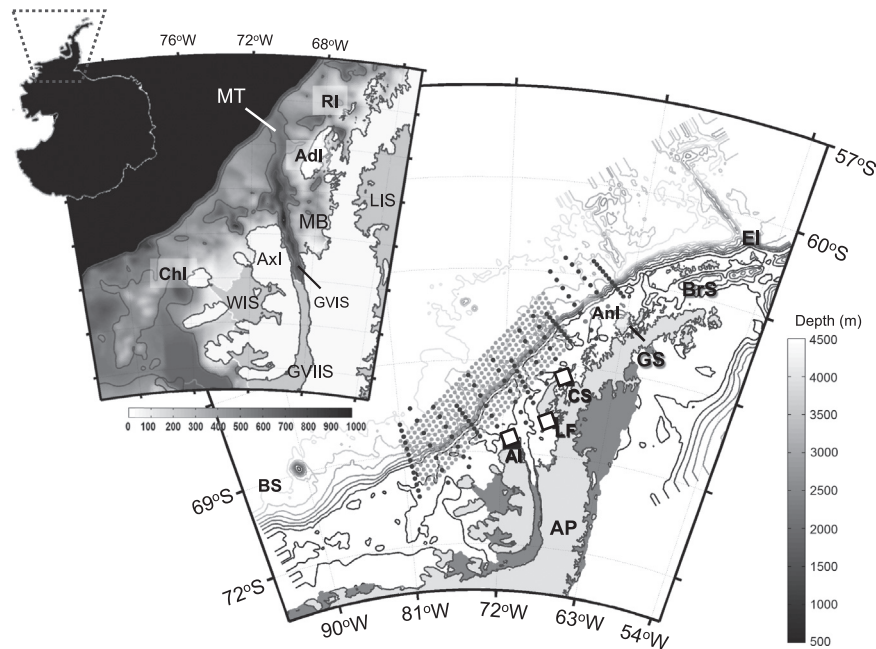
Fig. 1. (A) Map of the study area showing the western Antarctic Peninsula (wAP) continental shelf region and bottom bathymetry. (B) Release sites for the Lagrangian particle simulations (dark and light filled circles), and the biological hot spot regions (solid line box). Geographic names are abbreviated as EI—Elephant Island, BrS—Bransfield Strait, AnI—Anvers Island, GS—Gerlache Strait, RI—Renaud Island, CS—Crystal Sound biological hot spot, AdI—Adelaide Island, LIS—Larsen Ice Shelf, LF—Laubeuf Fjord hot spot, MT—Marguerite Trough, MB—Marguerite Bay, AI—Alexander Island biological hot spot, AxI—Alexander Island, GVIS—George VI Sound, AP—Antarctic Peninsula, GVIIS—George VI Ice Shelf, WIS—Wilkins Ice Shelf, ChI—Charcot Island and BS—Bellingshausen Sea.

waters. The latter observation suggested that the primary spawning region was along the outer portion of the wAP continental shelf (Siegel, 1988). The observed spatial separation of the krill maturity stages led Siegel (1988) to postulate a seasonal on–offshelf migration by Antarctic krill. Adult krill moved offshore in summer to spawn, after which they moved onshore to the inner portion of the shelf. This migration extended over distances of 50–100 km and occurred in 5–10 days (Kanda et al., 1982). The onshore adult migration was coincident with sea ice formation during fall, which provided a winter habitat for larvae (Daly, 2004) and resulted in larvae moving to the inner shelf region the next spring when the sea ice retreated (Siegel, 2000a; Nicol, 2003). This sequence is consistent with observed distributions of larval, juvenile, and adult krill (Siegel, 2000b) and observations of seasonal shifts in Antarctic krill biomass toward the inner wAP shelf (Lascara et al., 1999; Lawson et al., 2004, 2008; Ashjian et al., 2004; Ross et al., 2008; Wiebe et al., 2011).

During spawning Antarctic krill release embryos in the upper water column, which sink and hatch at depth (Marr, 1962; Quetin and Ross, 1984). The larvae swim to the surface where feeding begins. Successful completion of this descent–ascent cycle is subject to many constraints, one of which is the hatching depth of the embryo, which needs to be shallow enough for first larval feeding stage to reach the surface waters before depleting its carbon stores (Ross and Quetin, 1989).

Development and hatching of the embryo and larval swimming speed are accelerated at temperatures above 1 °C (Ross et al., 1988). Modeling studies of the descent–ascent cycle (Hofmann et al., 1992; Hofmann and Hüsrevoğlu, 2003) showed that the presence of Circumpolar Deep Water (CDW), a deep (300–500 m) water mass characterized by temperatures of 1.5–2 °C (e.g., Klinck (1998), Klinck et al. (2004)), accelerates embryo development and yields shallower hatching depths. At particular sites along the wAP shelf break, CDW moves onshelf flooding the region below 200 m with 1.5–2 °C water (Dinniman and Klinck, 2004; Klinck et al., 2004), which then mixes with the shelf waters (Moffat et al., 2009). The result is that much of the wAP continental shelf is

flooded with a modified version of CDW with temperatures of 1.0–1.5 °C (Klinck et al., 2004). The presence of this water and the deep (400–600 m, Bolmer, 2008) wAP shelf provide conditions that support successful completion of the descent–ascent cycle (Hofmann and Hüsrevoğlu, 2003).

Along the inner portion of the wAP continental shelf during fall and winter are regions characterized by enhanced biomass of Antarctic krill (Lawson et al., 2008) and top predator assemblages (Costa et al., 2007). These biological hot spot regions tend to be in areas that are influenced by CDW and numerical Lagrangian particle tracking studies suggest these regions have long residence times (Piñones et al., 2011, 2013); both of which potentially support enhanced local growth (Marrari et al., 2011). Lagrangian particle tracking simulations (Piñones et al., 2013) showed that these hot spot regions are maintained by inputs of Antarctic krill larvae from upstream areas, such as the western Bellingshausen Sea, as well as by retention by the local circulation.

Along the wAP, warming of atmospheric (Vaughan et al., 2003) and ocean water (Meredith and King, 2005) temperatures has been observed and sea ice extent and duration has changed (Stammerjohn et al., 2008a). These changes have been attributed to various processes, one of which is the Southern Annular Mode (SAM), the primary mode of atmospheric variability over the Southern Ocean (Marshall, 2003). During the past few decades, there has been a shift toward a positive SAM (Thompson et al., 2000) that has been related along the wAP to strengthening of the polar westerlies (Marshall et al., 2006), an increased frequency of mesoscale cyclones (Lubin et al., 2008) and a decrease in the extent and seasonal duration of sea ice (Liu et al., 2004; Stammerjohn et al., 2008b). The consequences of these changes for Antarctic krill are unknown.

The first objective of this study was to identify regions of the wAP continental shelf that support successful completion of the descent–ascent cycle and to determine the relationship of these regions to spawning and hot spot regions. The second objective was to determine how the areas of successful reproduction may be modified by climate-induced changes in environmental

conditions. The first objective was addressed using a one-dimensional, temperature-dependent model that simulates the descent–ascent cycle of the embryos and early larval stages of Antarctic krill (Hofmann et al., 1992; Hofmann and Hüsrevoğlu, 2003) and Lagrangian particle simulations obtained from a numerical circulation model implemented for the wAP continental shelf (Dinniman and Klinck, 2004; Dinniman et al., 2011). The second objective was addressed with simulations that used modified temperature and circulation patterns produced by expected changes in wind speed and transport of the Antarctic Circumpolar Current (ACC) resulting from climate variability along the Antarctic Peninsula (Dinniman et al., 2012).

The models used in this study are described in the next section. This is followed by simulation results from the descent–ascent cycle model and Lagrangian particle simulations that were obtained for present and modified temperature conditions. The discussion section summarizes these results in terms of the effects of the circulation, residence times and current understanding of Antarctic krill distributions on the wAP continental shelf.

2. Methods

2.1. Embryo–larvae descent–ascent model

The model that simulates the descent of an Antarctic krill embryo and ascent of the larva is described in detail in Hofmann et al. (1992) and Hofmann and Hüsrevoğlu (2003) and only a general description is given here. The embryo sinking velocity depends on developmental stage, and ambient water temperature and density. The time-dependent sinking rate ($Sr(t)$, m s^{-1}) of the embryo is given by

$$Sr(t) = \frac{Dm^2}{18\nu} g \left(\frac{\rho_e}{\rho_w} - 1 \right) \quad (1)$$

where Dm is the diameter of the embryo (μm), ν is the kinematic viscosity of water (1.787×10^{-6} m^2 s^{-1}), g is the gravitational acceleration, ρe is the density of the embryo and ρw is the density of the ambient sea water (both in g cm^{-3}).

The embryo changes its initial diameter (Dm_0) as it develops through five embryonic stages that are defined as single cell to early gastrula (SC–eG), early gastrula to gastrula (eG–G), gastrula to early limb bud (G–eLB), early limb bud to late limb bud (eLB–lLB) and late limb bud to hatch (lLB–NI). The temperature-dependent developmental time (days) for the embryonic stages (De) was obtained from empirically-derived relationships

$$De_i(T) = \begin{cases} 1.225e^{-2.351T} + 24.147 & \text{for SC to eG} \\ 33.3 - 10T \quad \text{if } T \text{ is } < 0^{\circ}\text{C} & \text{for eG to G} \\ 33.3 \qquad \text{if } T \text{ is } \geq 0^{\circ}\text{C} & \text{for eG to G} \\ 11.851e^{-1.123T} + 62.404 & \text{for G to eLB} \\ 110.15 - 14.8T & \text{for eLB to lLB} \\ 37.258e^{-0.907T} + 108.644 & \text{for lLB to NI} \end{cases} \quad (2)$$

where i designates the different embryonic stages. The developmental time obtained from Eq. (2) represents the time from spawn to the end of the indicated stage. The change in embryo diameter depends on temperature and developmental stage

where fD is the fraction of the embryonic development that has been completed and T is the ambient water temperature (°C). The fraction of embryonic development is computed at each model time step (1 h) relative to the total development time for a given stage (obtained from Eq. (2)). The initial diameter of the embryo (Dm_0) used in this study was 620 μm (Hofmann et al., 1992). Sensitivity studies of the effect of the initial embryo diameter showed that diameters greater than 626 μm produced a positively buoyant embryo during the late gastrula stage and those less than 622 μm resulted in a rapidly sinking embryo; neither of which agrees with observations (Hofmann and Hüsrevoğlu, 2003). The initial diameter used in this study is within the ± 10 μm precision of the initial diameters measurements reported by Quetin and Ross (1984).

The density of the embryo was calculated from the wet weight (Ww) and the diameter of each developmental stage (i) as

$$\rho_e = \frac{6Ww_i}{\pi Dm_i^3} \quad (4)$$

where wet weight was calculated from the embryo diameter as

$$Ww_i(Dm) = \begin{cases} 0.6146Dm - 250.4528 & \text{for SC to eG} \\ 0.4963Dm - 175.1451 & \text{for eG to eLB} \\ 0.7539Dm - 340.0911 & \text{for eLB to lLB} \\ 0.7099Dm - 311.4229 & \text{for lLB to NI} \end{cases} \quad (5)$$

After the embryo hatches, the larva ascends with an ascent rate (Ar, m s^{-1}) that depends on ambient temperature as

$$Ar(t) = \begin{cases} -(0.011T + 0.208)Ps & \text{if } T < 0^{\circ}\text{C} \\ -(0.043T + 0.208)Ps & \text{if } T \geq 0^{\circ}\text{C} \end{cases} \quad (6)$$

where Ps is the fraction of time the larvae spends swimming, which was set to 30% (Hofmann et al., 1992; Hofmann and Hüsrevoğlu, 2003). Hofmann et al. (1992) determined this value by comparisons between the simulated depths of various larval stages with observed depths from trawls data (Hempel and Hempel, 1986). The 30% value produced simulated depth distributions that agreed with observations. Additional analysis of the sensitivity to the fraction of time the larvae spend swimming (Hofmann and Hüsrevoğlu, 2003) showed that reducing the fraction to 20% resulted in more larvae reaching the surface as calyptopis 1 and 2, which does not agree with observed larval distributions. As the larva ascends it develops from nauplius (NI) through the metanauplius (MN) stages and into a calyptopis 1 (C1), the first feeding stage, and then into a calyptopis 2 (C2) stage. The development time (Dl) is temperature dependent and is calculated for each larval stage (i) from empirically-derived equations as:

$$Dl_i(T) = \begin{cases} 38.36e^{-1.41T} + 225.29 & \text{for NI to MN} \\ 78.26e^{-1.53T} + 417.93 & \text{for NI to C1} \\ 320.58e^{-1.1T} + 752.22 & \text{for NI to C2} \end{cases} \quad (7)$$

During the descent the embryo respires and the metabolic cost of this is covered by the internal carbon stores that the embryo has upon spawning. Similarly, respiration costs during ascent when the larva is not feeding are covered by the internal carbon stores. Embryo and larval respiration rates (μlO$_2$ h^{-1}), are dependent on

$$Dm_i(fD) = \begin{cases} Dm_0 + 6.605 + 104.936fD - 247.258fD^2 + 192.003fD^3 & \text{if } T < 0^{\circ}\text{C} \\ Dm_0 + 1.557 + 153.305fD - 355.408fD^2 + 260.204fD^3 & \text{if } 0^{\circ}\text{C} \leq T < 1^{\circ}\text{C} \\ Dm_0 + 0.460 + 150.220fD - 334.003fD^2 + 238.811fD^3 & \text{if } 1^{\circ}\text{C} \leq T < 2^{\circ}\text{C} \\ Dm_0 + 1.505 + 138.389fD - 325.546fD^2 + 260.204fD^3 & \text{if } 2^{\circ}\text{C} \leq T \end{cases} \quad (3)$$

the fraction of total development (fD) and are given by

$$R_{embryo} = 0.8368 \times 10^{0.7195fD}$$

$$R_{larva} = 11.1030 \times 10^{0.8489fD} \qquad (8)$$

The carbon used by the embryo and larva was calculated using a standard conversion constant of 0.385 μg carbon used per 1 μl of oxygen consumed (Quetin and Ross, 1989; Hofmann et al., 1992). The initial carbon content for the embryo (15 μg carbon) must sustain the embryo during its descent and the larva during the ascent until it reaches the C1 first feeding stage (Ross and Quetin, 1989). The point of no return (the starvation threshold) for C1 was 7.5 μg carbon (Ross and Quetin, 1989; Hofmann et al., 1992).

The descent–ascent model was implemented using temperature and density fields obtained from the wAP numerical circulation model (see following section) for the time corresponding to the Antarctic krill reproductive season, which extends from December to March (Ross and Quetin, 1986; Spiridonov, 1995). The simulated temperature and density fields extend from 1 January 2000 through December 2002 (Dinniman et al., 2012).

The diagnostics calculated from the descent–ascent model were the vertical displacement of the embryo–larvae particle in the water column, the development time from hatching to C2, and carbon usage. An assumption made in implementing the descent–ascent cycle is that the embryo can complete development on the bottom, similar to Hofmann et al. (1992) and Hofmann and Hüsrevoğlu (2003). However, for assessing the potential effects of modified environmental conditions, only the shelf areas with bottom depths greater than the hatching depth were considered as suitable habitat for completion of the descent–ascent cycle.

2.2. Circulation model and Lagrangian particle tracking

The numerical circulation model is based on an implementation of the Regional Ocean Modeling System (ROMS) version 3.0 for the wAP region (Dinniman et al., 2012). This model is a free-surface, terrain-following, primitive equations ocean circulation model (Haidvogel et al., 2008; Shchepetkin and McWilliams, 2009). The circulation model was coupled to a dynamic sea-ice model (Budgell, 2005) and thermodynamically active ice shelves (Dinniman et al., 2007). The model domain extended along the western side of the Antarctic Peninsula from 72°S to the tip of the Peninsula, covered the entire continental shelf, and extended about 500 km offshore from the shelf break (Fig. 1). The horizontal grid spacing was 4 km and there were 24 vertical levels, which were concentrated toward the top and bottom of the domain. Wind forcing was done using 6-hourly winds, distributed on a 1/2° grid, obtained from a blend of QuikSCAT scatterometer data and

National Centers for Environmental Prediction analyses (Milliff et al., 2004), as described in Dinniman et al. (2012), for the years 2000–2002. The model was initialized in 15 September and run for over four years with a two year cycle of repeated winds. Further details of the wAP circulation model bathymetry, initial and boundary conditions, as well as, evaluations of the simulated circulation distributions are given in Dinniman and Klinck (2004), Dinniman et al. (2011, 2012).

The transport of the early life stages of Antarctic krill was simulated using Lagrangian particle tracking experiments embedded in the wAP circulation model. The wAP circulation model provided current fields (u, v and w components of the flow), that were used to simulate the trajectory followed by a particle ($\vec{X}$) in space (x, y, z) and time (t), described as

$$\frac{d\vec{X}}{dt} = \vec{U}(\vec{X}, t) + W_{vw}\hat{Z} \qquad (9)$$

where $d\vec{X}/dt$ is the change of the location of the particle in the three-dimensional field with time. The location is modified by the advective velocity field ($\vec{U}(\vec{X}, t)$), obtained from the circulation model, and vertical diffusivity ($< 10^{-2}$ m^2 s^{-1}), which was included by adding a vertical random walk to the particle location. The random vertical displacement (W_{vw}) was added to the vertical ($\hat{Z}$) particle location at each time step (Hunter et al., 1993; Visser, 1997).

The numerical integration for the Lagrangian circulation was done using a fourth-order Milne predictor (Abramowitz and Stegun, 1964) and a fourth-order Hamming corrector scheme (Hamming, 1973). A forward difference scheme was used when vertical displacement resulting from vertical walk parametrization was estimated. The vertical displacement has a Gaussian probability distribution and there is a correction for the vertical gradient in the diffusion coefficient. A 4-min integration time was used for the Lagrangian particles, which is the same as the baroclinic integration time. The location of each particle was obtained at 12-h intervals, which is smaller than the temporal decorrelation scales estimated for the circulation on the wAP continental shelf (Piñones et al., 2011). Mesoscale eddies on the wAP shelf ($\sim$10 km) are not adequately resolved by the 4-km horizontal resolution of the circulation model. However, observations (Moffat et al., 2009) show that these eddies have small cross-stream velocities (0.01–0.05 m s^{-1}) compared with simulated (Dinniman et al., 2011) and observed (Savidge and Amft, 2009) mean advective currents ($\sim$0.10–0.20 m s^{-1}), and thus are not a significant contributor to particle dispersion (Piñones et al., 2013).

This study considers neutrally buoyant particles. An assessment of the effect of vertical migration on transport patterns and times

Table 1
Summary of the simulations with the embryo–larva model and the circulation–Lagrangian particle tracking model. The environmental conditions, release locations and release frequency used in each simulation are given.

Simulation	Model configuration	Environmental conditions	Release location	Depth (m)	Number of release points	Frequency	Length of simulation (days)
Set 1—descent–ascent model	Embryo–larvae model	Present	Each grid point	24-sigma levels	100,786	Austral Summer	15–35
Set 2—hot spots	Circulation model–Lagrangian particles	Present	Across-shelf exchange sites	0, 50, 100, 150, 200, 250, 300	113	23 January–14 March at 10-day intervals	760
Set 3—shelf aggregation	Circulation model–Lagrangian particles	Present	High resolution (4-km) grid, along shelf break	300	407	23 January–14 March at 10-day intervals	1270
Set 4—descent–ascent model	Embryo–larvae model	Modified	Each grid point	24-sigma levels	100,786	Austral Summer	15–35
Set 5—hot spots	Circulation model–Lagrangian particles	Modified	Across-shelf exchange sites	0, 50, 100, 150, 200, 250, 300	113	23 January–14 March at 10-day intervals	760
Set 6—shelf aggregation	Circulation model–Lagrangian particles	Modified	High resolution (4-km) grid, along shelf break	300	407	23 January–14 March at 10-day intervals	1270

for the Lagrangian particles showed that this process made less than 10% difference in the horizontal and vertical dispersion of particles (Piñones et al., 2013) because the flow velocities on the wAP shelf are typically less than 0.05 m s^{-1} and vertical density gradients are weak (Dinniman and Klinck, 2004). The simulated particle trajectories were compared with trajectories from World Ocean Circulation Experiment (WOCE)-style drifters deployed along the wAP continental shelf and were found to be representative of general transport times and pathways (Piñones et al., 2011).

2.3. Descent–ascent cycle and Lagrangian particle experiments—present conditions

The first set of simulations (Table 1) focused on the embryo–larva descent–ascent model (Eqs. (1)–(8)). These simulations used seasonal mean sea water temperature (Fig. 2) and density

(not shown) fields obtained from the wAP circulation model as inputs to the descent–ascent cycle model, which was implemented at each grid point used for the circulation model. The vertical trajectories from these simulations provided estimates of embryo hatching depths along the wAP continental shelf and larval ascent times.

The second set of simulations (Table 1) focused on particles that were released on the wAP shelf (configuration and release locations shown in Fig. 1—dark filled circles; also see Piñones et al. (2011)) in a pattern that was designed to determine primary transport pathways and residence times for three shelf areas that are characterized by enhanced biological production (biological hot spots, Costa et al., 2007). As part of these simulations, particles were released in transects across the shelf break, between 0 and 300 m at 50-m intervals, in regions where CDW intrusions are observed (Fig. 1). The transport times obtained from the Lagrangian experiments were mapped to
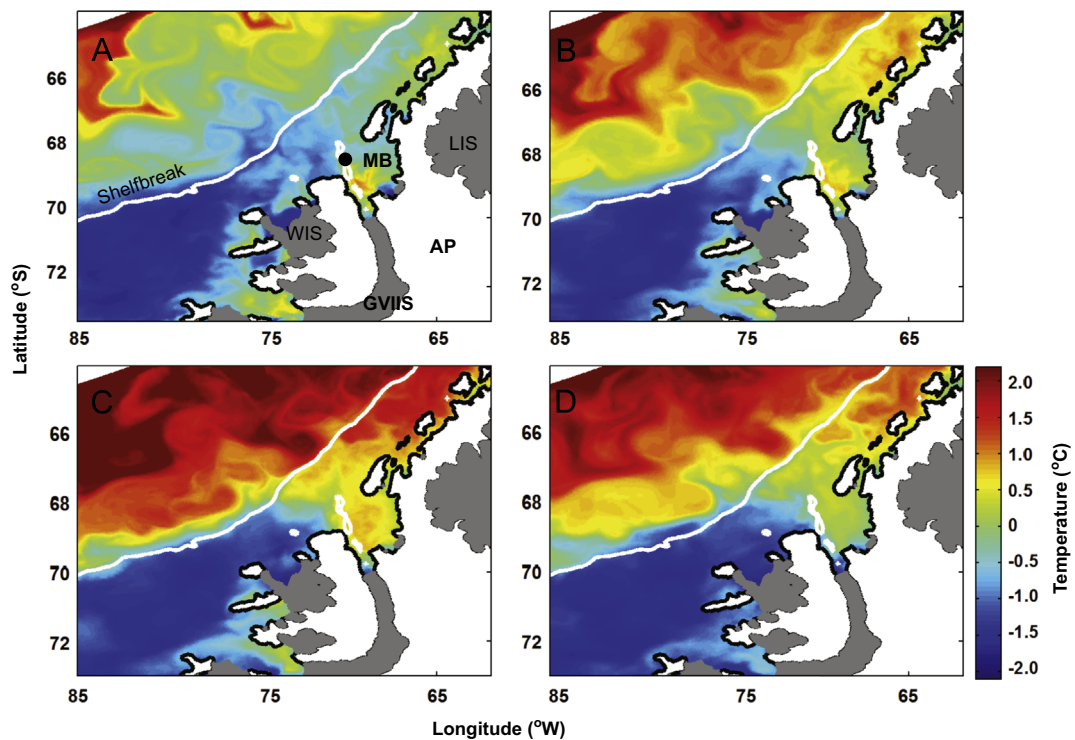

Fig. 2. Monthly-averaged simulated sea surface temperature distribution for (A) December, (B) January, (C) February, and (D) March. The 800-m isobath (white line) indicates the location of the shelf break and the deep areas along Marguerite Trough. The location of the vertical profiles shown in Fig. 3 is indicated (black filled circle). Geographic names are abbreviated as LIS—Larsen Ice Shelf, MB—Marguerite Bay, AP—Antarctic Peninsula, GVIIS—George VI Ice Shelf and WIS—Wilkins Ice Shelf.

Table 2
Duration (days) of the cumulative developmental time of krill larvae obtained from laboratory experiments, field data analysis, and modeling studies. The development times obtained from modeling studies represent average conditions during the reproductive season (December–March). Antarctic krill life stages are abbreviated as N=Nauplius (stages 1–2), MN=Metanauplius, C=Calyptopis (stages 1–3), F=Furcilia (1–6).

Source	Stage											
	N1	N2	MN	C1	C2	C3	F1	F2	F3	F4	F5	F6
Witek et al. (1980)[a]	–	–	–	30	45–60	60–75	70–90	75–105	90–120	105–135	120–180	135–240
Ikeda (1984)[b]	8	13	20	30	44	52–55	63–64	75	85–87	98–102	111–114	124–131
Ross et al. (1988)[a,b]	–	14–24	22–41	38	52	–	–	–	–	–	–	–
Daly (1990)[a,b]	–	–	–	–	–	–	–	–	90–121	95–135	118–164	114–193
Hofmann et al. (1992)[c]	5–8	–	10–16	18–33	33–45	–	–	–	–	–	–	–
Hofmann and Lascara (2000)[c]	–	–	–	32	44	50	58	70	100	117	163	258
Duration	5–8	13–24	10–41	18–38	33–60	50–75	58–90	70–105	85–121	95–135	111–180	114–258
Median	7	19	26	28	47	63	74	88	103	115	146	186

[a] Field data analysis.
[b] Laboratory experiments.
[c] Modeling studies.

Antarctic krill developmental times using data from observations, modeling and laboratory experiments (Table 2).

The third set of Lagrangian simulations (Table 1) consisted of particle releases at 300 m in a high resolution grid (every 4 km) along the shelf break at 10-day intervals starting 23 January (Table 1, Fig. 1—light filled circles). The frequency distribution of particles along the shelf was estimated by the arrival of particles in regions of 8 km × 8 km along the shelf for the region that extends from west of Charcot Island to Elephant Island at the tip of the Antarctic Peninsula (Fig. 1). The number of particles in each area was recorded at 10-day intervals for a total of 3.5 years. The frequency distribution of particles along the shelf provided esti-mates of areas that favor aggregation and retention of particles. Lagrangian particle experiments (second and third simulation sets, Table 1) were initialized on 23 January, which allows comparisons with Lagrangian simulations given in Piñones et al. (2011) that used present environmental conditions and corresponded to the peak spawning period in the Marguerite Bay and Bellingshausen Sea regions (Spiridonov, 1995)

2.4. Descent–ascent cycle and Lagrangian particle experiments—modified conditions

The fourth set of simulations (Table 1) used the embryo–larvae descent–ascent model and temperature and density distributions obtained from the wAP circulation model that was forced with modified atmospheric and oceanographic conditions. These mod-ifications consisted of increased wind speed (i.e., the westerlies) and increased transport of the ACC, both of which affect the

volume of CDW transported onto the wAP continental shelf (Dinniman et al., 2012). These modified conditions, resulted in increased advection of warm water (heat) to the upper-shelf waters and a reduction in sea ice extent (Dinniman et al., 2012). For these simulations, the present day winds (1 January 2000–31 December 2002) were scaled by a constant factor, which increased wind speed by 20% and the ACC transport was increased by 6% by imposing a stronger salinity gradient along the locations where the Southern ACC Front enters the model domain (Dinniman et al., 2012). The increase in wind speed is based on observations of poleward intensification of westerly winds (Thompson and Solomon, 2002; Marshall et al., 2006) and projected increases in westerly strength from a coupled climate model (Bracegirdle et al., 2008).

The final sets of simulations used the release sites and frequen-cies from the present-condition Lagrangian simulations (Fig. 1, Table 1) with the modified circulation distributions. Differences in particle transport patterns (modified – present conditions) pro-vide an estimate of variability in source regions for the biological hot spot regions and larval fate. Summer averages of residence times were estimated for the biological hot spots regions under present and modified conditions. Residence times were obtained by releasing one particle at each grid point in a 24 km × 24 km grid between 0 and 300 m at 50-m intervals, for a total of 343 particles in every hot spot (Fig. 1). The position of the particle is obtained every 12 h; the time required for the particles to exit the release area was taken as a measure of the residence time for the region. Further details of the calculation of residence times is given in Piñones et al. (2011)
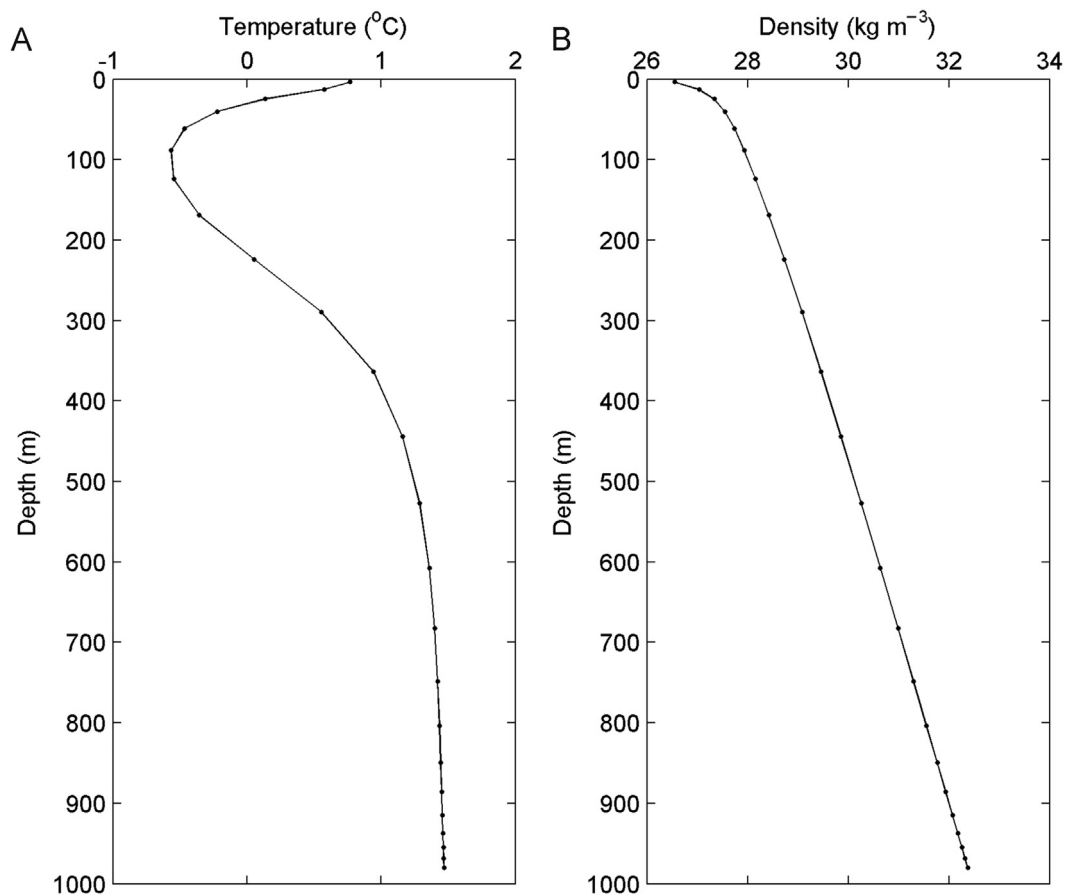

Fig. 3. Simulated vertical distribution of (A) potential temperature and (B) density anomaly from a site at Marguerite Bay on the wAP continental shelf (location shown in Fig. 2). These austral summer (December–March) mean profiles were obtained from the present day circulation simulation. The filled circles correspond to the layers used in the wAP circulation model.

3. Results

3.1. Temperature and density

The mean simulated surface temperature obtained using the present day atmospheric and oceanographic forcing for the months corresponding to the Antarctic krill reproductive season showed that warming begins in the southwestern inner portion of Marguerite Bay in December and progresses northward (Fig. 2A, B). The maximum surface temperatures (1–2 °C) occurred in February (Fig. 2C). By March, surface temperatures in Marguerite Bay had cooled to just above 0 °C. Surface temperatures in regions outside and to the north of Marguerite Bay remained above 1 °C. Simulated surface density remained relatively constant (1027–1027.5 kg m^{-3}) along the shelf from December to March (not shown). The minimum densities (1025.5–1026.0 kg m^{-3}) were observed onshore, southwest of Alexander Island.

The mean simulated vertical temperature and density profiles (Fig. 3) from a site in Marguerite Bay (Fig. 2A) show that the wAP circulation model reproduced the water mass structure for this region. Antarctic Surface Water (AASW), characterized by potential temperatures between −1.8 and 1.0 °C (Fig. 3A) and density anomalies < 27.4 kg m^{-3} (Fig. 3B), is present in the upper 80–100 m, as observed (Klinck et al., 2004). The simulated temperature minimum, which indicates Winter Water (WW), occurs below the AASW between 100 and 200 m, which is in agreement with observations from the Marguerite Bay region (Klinck et al., 2004). Below WW, the shelf is flooded with a modified form of CDW,

which is characterized by temperatures above 1 °C (Klinck et al., 2004) and this pattern is seen in the simulated vertical distributions (Fig. 3A). Comparisons of the simulated circulation and temperature distributions to observations indicate good agreement in surface temperature and the vertical distribution of water masses (Dinniman and Klinck, 2004; Dinniman et al., 2011, 2012.

3.2. Descent–ascent cycle, hatching depth, and retention—present conditions

The simulated hatching depth was relatively uniform at 400–600 m along and beyond the shelf break (Fig. 4A), which is shallower than the bottom depth. The descent–ascent cycle over the wAP shelf resulted in hatching depths of 450–700 m (Fig. 4A). Hatching depths in the Crystal Sound region were shallower at 400–670 m (Fig. 4A and E), and for most of the region are above the bottom (Fig. 1B). Hatching depths in the southwestern part of the wAP shelf were between 400 and 700 m (Fig. 4A and B), which are above the bottom depth for much of this region (Fig. 1B). Over Marguerite Trough where depths are more than 900 m, the embryo hatched at 600 m and the descent–ascent cycle was completed in 15 days (Fig. 4A and C). At the Laubeuf Fjord site inside Marguerite Bay, the embryo reached the bottom (620 m) and completed hatching after 24 h on the bottom (Fig. 4D). In the shallow inner shelf regions, the hatching depth was the same as the bottom depth, 200 m or shallower (Fig. 4A), and the embryo hit the bottom before hatching. In these regions the embryo spent 3–5 days on the bottom before hatching.
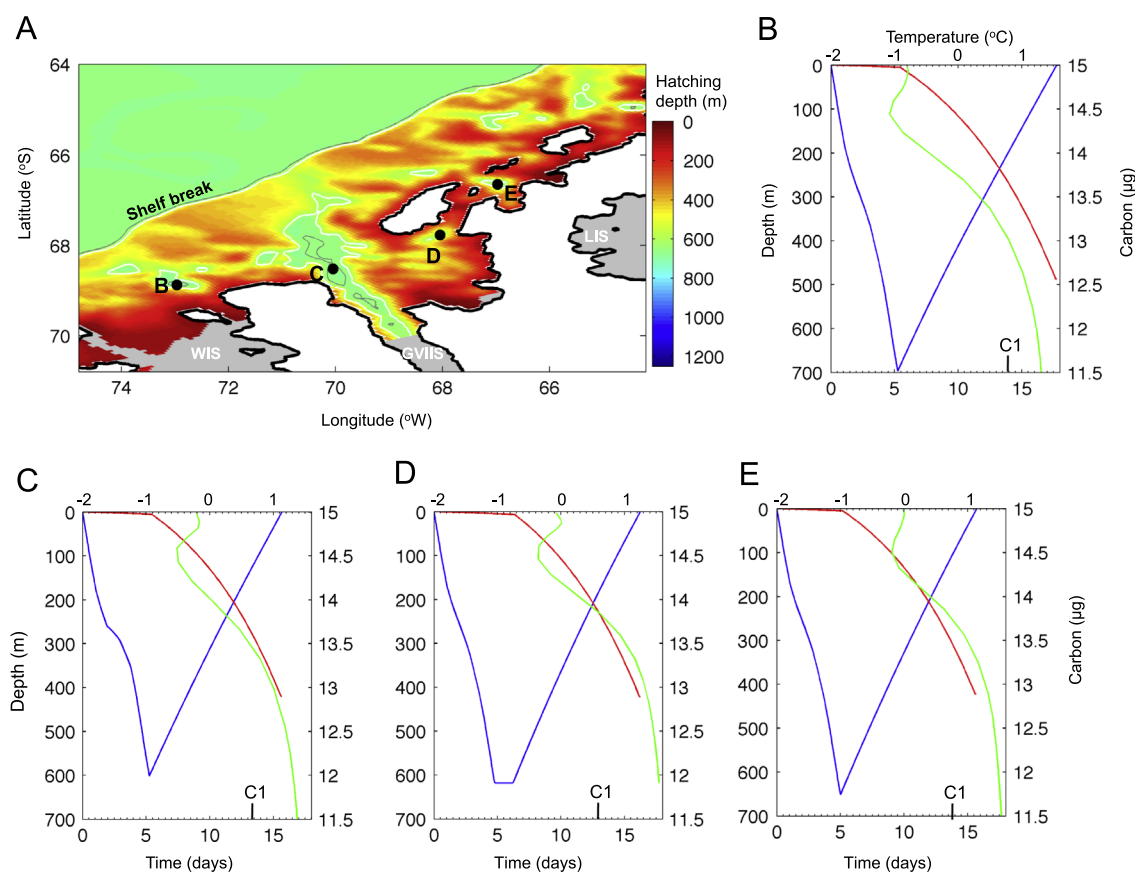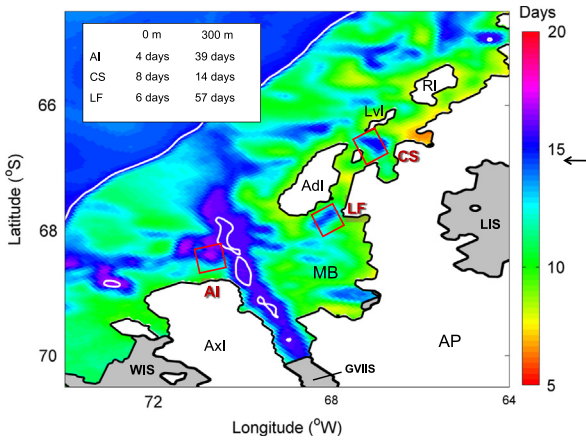

Fig. 4. Distribution of simulated hatching depths for krill embryos released over the wAP continental shelf at each grid point of the circulation model and the location of the vertical profiles (black circle) shown in panels B–E (A). Simulated vertical trajectories (blue line), remaining internal carbon stores assuming no feeding during calyptopis 1 (red line) and vertical potential temperature (green line) distributions obtained for embryo–larva particles released (B) west of Alexander Island, (C) in Marguerite Trough, (D) in Laubeuf Fjord, and (E) in Crystal Sound. Development to calyptopis 1 is indicated by C1. Geographic names are abbreviated as LIS—Larsen Ice Shelf, AP—Antarctic Peninsula, GVIIS—George VI Ice Shelf and WIS—Wilkins Ice Shelf. The 800-m isobath is indicated (solid gray line). (For interpretation of the references to color in this figure legend, the reader is referred to the web version of this article.)

The sinking velocity of the simulated embryo depends on development, which is temperature dependent. As a result, the simulated sinking rates obtained for various locations on the wAP continental shelf were variable (Fig. 4B–E). Initial sinking rates
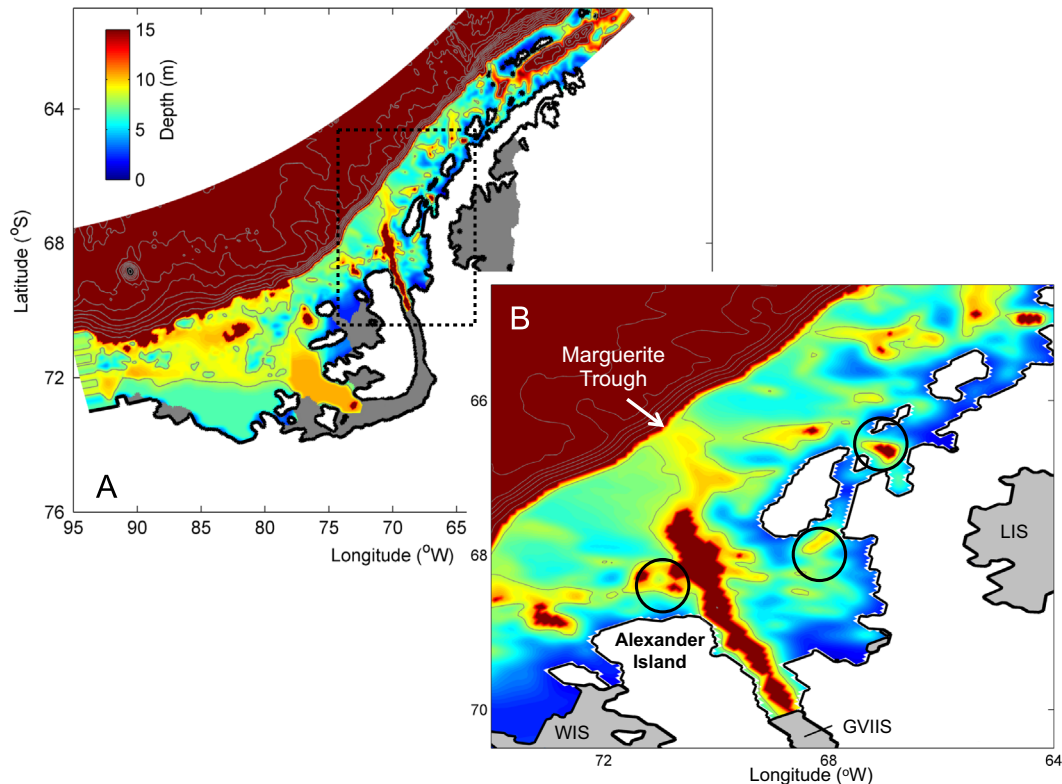

Fig. 5. Time (days) required for the simulated embryo–larvae particles to complete the descent–ascent cycle. The time required for development to the calyptopis 1 in the Alexander Island (AI), Crystal Sound (CS) and Laubeuf Fjord (LF) hot spot regions (red boxes) is indicated by the arrow. The inset table shows the residence times for particles at the surface and 300 m obtained from the Lagrangian simulations given in Piñones et al., (2011). The 800-m isobath (white line) shows the location of the shelf break and deep areas along the shelf. Geographic names are abbreviated as RI—Renaud Island, LvI—Lavoiser Island, CS—Crystal Sound hot spot, AdI—Adelaide Island, LF—Laubeuf Fjord hot spot, LIS—Larsen Ice Shelf, MB—Marguerite Bay, AI—Alexander Island hot spot, AxI—Alexander Island, AP—Antarctic Peninsula, GVIIS—George VI Ice Shelf and WIS—Wilkins Ice Shelf. (For interpretation of the references to color in this figure legend, the reader is referred to the web version of this article.)

were fast, 185–190 m day^{-1}, which moved the embryo to about 250 m in 2–3 days (Fig. 4B–E). The sinking rate slowed 2–3 days after release when the embryo reached the gastrula stage. This reduction in sinking rate retained the embryo in the upper part of CDW for 3–4 days where developmental rate increased (Fig. 4B–E). During the last 2–3 days of embryonic development, the sinking rate again increased to 181–186 m day^{-1}. Hatching depths ranged from 600 m and 700 m (Fig. 4A). Following hatching the larva ascended, reaching the sea surface in 10–13 days. The simulated carbon content showed that the internal carbon stores of the spawned embryo were sufficient to sustain the embryo and larvae throughout its descent and ascent.

Embryos spawned inside Marguerite Bay completed the descent–ascent cycle in approximately 14–15 days (Fig. 4C and D). The embryo portion of the cycle took 4–5 days and hatching occurred around 600 m, which is above or just at the bottom for most of this region (Fig. 1B). Larval ascent took about 10 days and the larva reached the surface as the first feeding stage. South of Marguerite Bay the descent–ascent cycle took approximately 3 additional days (Fig. 4B). Water temperatures in this area are 0.5 °C colder (Fig. 4B) than those for the locations in Marguerite Bay, which slowed the embryo development and hence sinking rate and resulted in hatching at about 700 m (Fig. 4B). The ascent time was also longer (Fig. 4B). The Crystal Sound region on the inner shelf north of Marguerite Bay supported completion of the descent–ascent cycle in 15.5 days (Fig. 4E). This region of the wAP continental shelf has warmer temperatures in the upper water column and is influenced by warm CDW below 200 m (Fig. 4E).

The time required for an embryo–larvae particle to reach C1 was 13–15 days along Marguerite Trough and in the deeper regions of the wAP continental shelf (Fig. 5). In the biological hot spot regions, development from embryo to C1 took 14–15 days

Fig. 6. Depth difference (m) between the simulated embryo hatching depth and the (A) wAP continental shelf bathymetry and (B) Marguerite Bay bathymetry (region outlined by box in (A)). Only differences of up to 15 m are indicated (dark red) because of the large differences associated with the deeper waters off the shelf. The locations of biological hot spots (black circles) and bathymetry contours at 500-m intervals (gray lines) are shown. Geographic names are abbreviated as LIS—Larsen Ice Shelf, AP—Antarctic Peninsula, GVIIS—George VI Ice Shelf and WIS—Wilkins Ice Shelf. (For interpretation of the references to color in this figure legend, the reader is referred to the web version of this article.)

(Fig. 5). The bathymetry and circulation of these regions favor retention; especially below 200 m. Residence times for particles at 300 m are longer than those at surface (inset table, Fig. 5). In the shallow shelf regions, the descent–ascent cycle was completed in 10 days or less (Fig. 5). However, most of the embryo development occurred after it hit the bottom. The larval ascent time was shortened to 4 to 6 days because of the shallow water column.

Throughout the wAP mid-shelf the bottom depth exceeds hatching depth by 10–15 m at several locations (Fig. 6), which allows embryos to hatch above the seabed. Along the inner shelf some regions where the difference is more than 10 m occur, but these are limited in extent (Fig. 6A). Within the Marguerite Bay region, areas where the bottom depth exceeds the embryo hatching depth occur along Marguerite Trough and in the biological hot spot regions (Fig. 6B). Smaller additional regions occur on mid-shelf off Alexander Island and southwest of Charcot Island and off the northern end of Adelaide Island (Fig. 6B). The regions of the wAP continental shelf where bathymetry does not constrain the descent–ascent cycle are offshore of the shelf break, in Bransfield Strait at the northern tip of the Antarctic Peninsula, and an area south of Elephant Island (Fig. 6A).

The bathymetry and circulation of the biological hot spot regions favors retention, especially below 200 m (inset table, Fig. 5). The residence times for the Alexander Island and Laubeuf Fjord areas, determined from Lagrangian particle tracking simulations, are almost 3–4 times the required time to complete

development to C1. The average residence time for the Crystal Sound biological hot spot region was 14 days (Fig. 5), which is approximately equivalent to the time required to complete the descent–ascent cycle at this location (Fig. 5A).

3.3. Descent–ascent cycle, biological hot spots, and sea ice distribution—modified conditions

3.3.1. Modifications to the descent–ascent cycle

The simulated hatching depths obtained using temperature and density distributions from the modified circulation simulations showed little change from those obtained using present conditions (Fig. 7A and B). The largest differences occurred in Bransfield Strait along the southern side of the South Shetland Islands (Fig. 7A). The largest differences in the southern part of the wAP occurred along Marguerite Trough and in the Crystal Sound hot spot region where hatching depth shoaled by 10–20 m (Fig. 7B). Isolated regions of the wAP continental shelf showed increased hatching depths, but these were small relative to the overall shelf area (Fig. 7A and B). The difference in simulated embryo hatching time obtained for present and modified conditions showed little change over most of the mid and outer regions of the wAP continental shelf (Fig. 7C). The only region where faster development (3–5 days) occurred was in the inner shelf to the west and southwest of Alexander Island and along the shelf at 85°W. Two areas showed slight decreases (2–3 days) in embryo
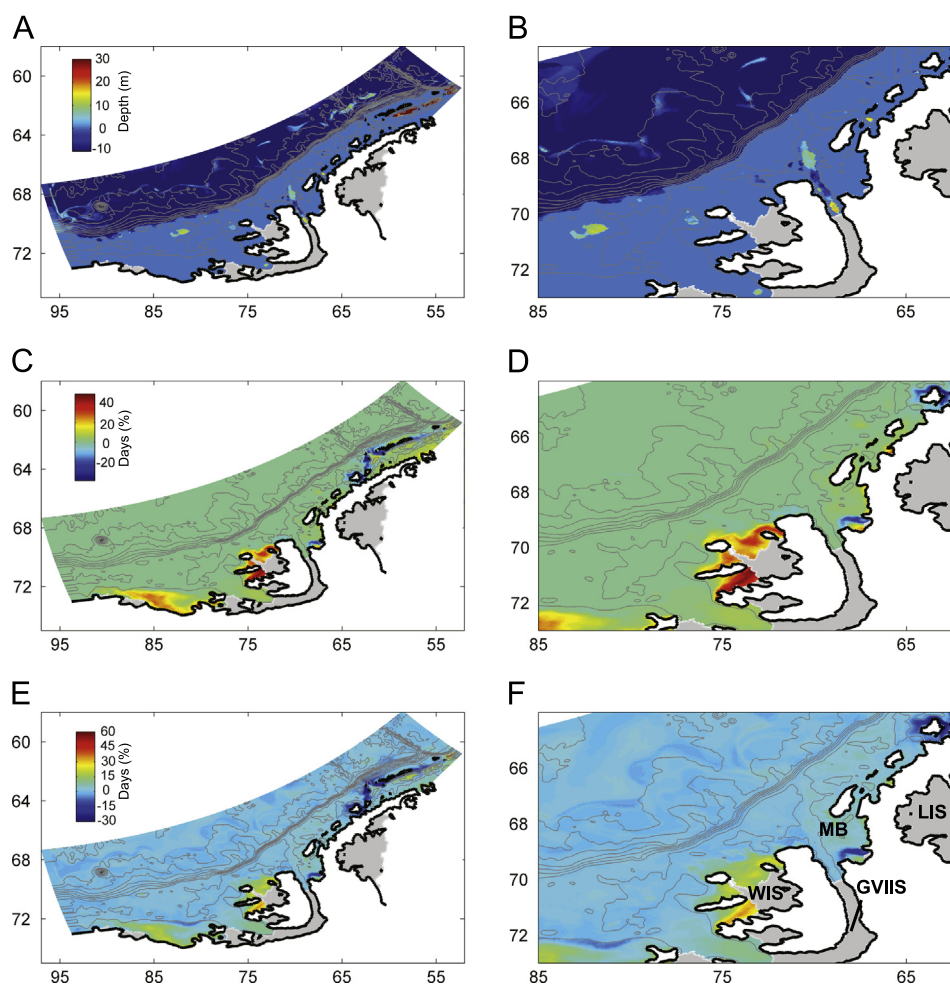
Fig. 7. Difference (modified minus present conditions simulations) for the entire wAP model domain (left panel) and Marguerite Bay region (right panel) for embryo hatching depth (A and B), time to complete the descent–ascent cycle (C and D), and embryo hatching time (E and F). Positive (negative) values indicate shallower (deeper) depths (A and B) and increased (decreased) time for embryo hatching and development (C–F). Geographic names are abbreviated as LIS—Larsen Ice Shelf, AP—Antarctic Peninsula, MB—Marguerite Bay, GVIIS—George VI Ice Shelf and WIS—Wilkins Ice Shelf.

development time (Fig. 7D), with the greatest decrease around Anvers Island and in a smaller region in the inner part of Marguerite Bay

Over the entirety of the wAP continental shelf the time required to complete the descent–ascent cycle differed only slightly between present and modified conditions (Fig. 7E). Faster cycle times occurred in the southern part of the wAP shelf near

Alexander Island; longer time occurred around Anvers Island (Fig. 7F).

### 3.3.2. Modifications to inputs to biological hot spots

Lagrangian particle tracking experiments that used the modified circulation distributions showed that the regions of the mid and outer wAP continental shelf that contribute to the Crystal Sound hot spot differed from those obtained for present conditions (Fig. 8A, D, G, Table 3). Inputs still originate in the Bellingshausen Sea region and along the shelf break; however, a larger percentage of particles were transported to this hot spot (40–80%) relative to what was obtained using present conditions (20–60%, Fig. 8G). The Alexander Island hot spot received inputs from the continental shelf area southwest of Marguerite Bay (Fig. 8B and E), similar to the inputs observed in the present conditions simulation (Fig. 8H). The modified circulation distributions resulted in additional inputs (40–60%) from regions along Marguerite Trough to the region off Alexander Island via common cyclonic transport pathway in Marguerite Bay (Fig. 8B and E). The Laubeuf Fjord region showed similar patterns of inputs for modified and present environmental conditions (Fig. 8C, F, I).

The modified circulation distribution favored particle aggregation in regions of the wAP shelf, which differs from the present hot spot regions, such as areas to the southwest off Alexander and

Table 3
Comparison of the mean residence time (days) and the percent contribution from particle source regions that provide inputs to each biological hot spot region obtained from simulations that used present and modified environmental conditions. The modified conditions consist of increased wind speed and increased transport of the ACC along the wAP continental shelf.

Hot spot region	Residence time (days)		Contribution (%) to hot spot	
	Present conditions	Modified conditions	Present conditions	Modified conditions
Crystal Sound	18.1	24.4	20–60	40–80
Laubeuf Fjord	30.9	39.1	20–40	40–60
Alexander Island	19.4	20.4	20–40	20–40
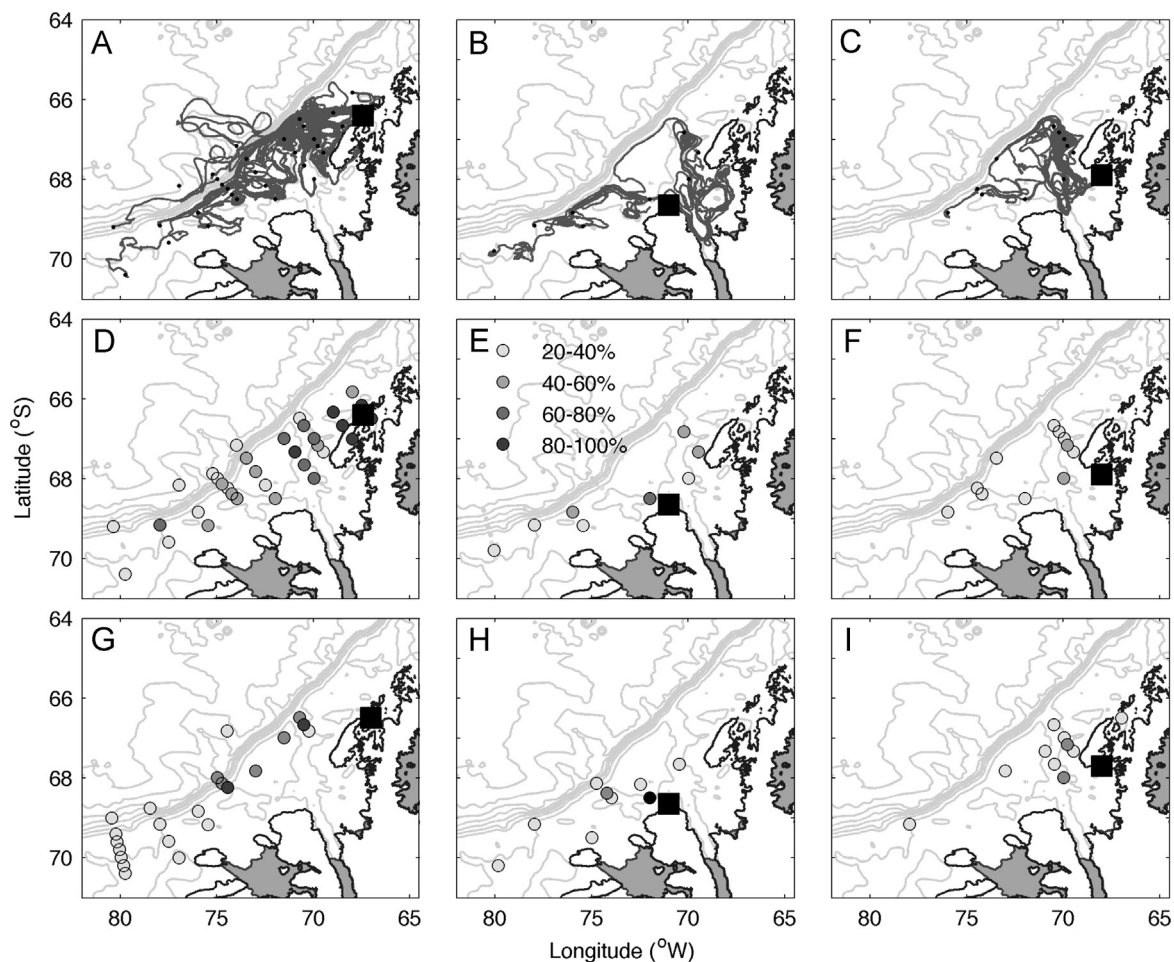
Fig. 8. Simulated particle trajectories (gray lines) and the distribution of the source regions and associated percentage of particles that were provided to the Crystal Sound (A, D, G), Alexander Island (B, E, H), and Laubeuf Fjord (C, F, I) biological hot spot regions (indicated by filled square) obtained using the modified circulation fields (A–F) and present circulation fields (G–I) Only the trajectories that originated in areas with contributions to the hot spots greater than 20% are shown. The simulated particles were released at 300 m (release point indicated by black dot) at 10-day intervals for 60 days in a grid of transects that extended across the continental shelf break (dark filled circles in Fig. 1(A), second set of simulations Table 1). The bottom bathymetry (m) from 500 m to 4000 m at 500-m intervals is shown by the light gray lines.

Charcot Islands (Fig. 9). The present hot spot area off Crystal Sound was enhanced by the modified conditions, with particle aggregation increasing by 15–20%. Areas along Marguerite Trough and present hot spot areas in Laubeuf Fjord and the mid and outer shelf off Renaud Island showed decreased (15%) particle aggregation with the flow obtained using the modified circulation fields.

The average residence times for the biological hot spots areas obtained for the modified environmental conditions were similar to those from the present conditions. The residence times for the Crystal Sound and Alexander biological hot spot region were approximately 20 days and approximately 40 days for Laubeuf Fjord (Table 3). These residence times are greater than the time required to complete development to C1.

3.3.3. Sea ice distribution

The difference in the summer average distribution of sea ice between modified and present conditions (Fig. 10A) showed reduced sea ice south and west of the Marguerite Bay. A 15–20% reduction was observed in a small region along the northwest side of Alexander Island and at the entrance of George VI Sound. The highest reduction was observed along the shelf west from Charcot Island toward the western Bellingshausen Sea region. The difference in the mean winter sea ice coverage between current and modified conditions (Fig. 10B) showed the largest reduction in sea ice along the inner shelf north of Marguerite Bay and along the mid and outer shelf west of Alexander Island. Sea ice reductions of 30% and 15% occurred in the hot spot regions of Crystal Sound and Laubeuf Fjord, respectively. The Alexander Island hot spot, and in general the inner shelf west of Charcot Island, showed a slight increase in sea ice cover (2–3%). Between Renaud Island and Gerlache Strait, the sea ice coverage decreased about 20%. Bransfield Strait also showed less sea ice cover (15% decrease).

Comparison with the Lagrangian particle trajectories (e.g., Fig. 8) showed that the areas with largest winter sea ice reductions are the same as those that provide particles to the biological hot spot regions (Fig. 11). The time scales of these particles are variable but are generally consistent with developmental times for krill larvae spawned along the mid and outer shelf, and toward the Bellingshausen Sea area (Fig. 11).
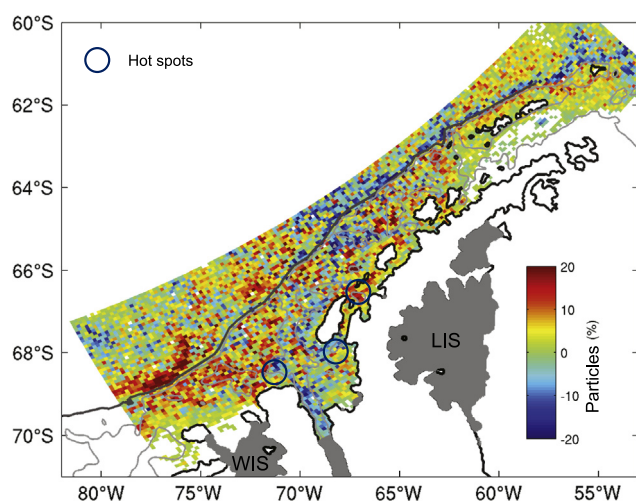
Fig. 9. Average percent difference (modified minus present conditions simulations) in the distribution of particles along the wAP continental shelf determined from an average of values obtained at 10-day intervals for 3.5 years. Positive (negative) values indicate a higher (lower) percentage of particles per area for the modified circulation conditions. The 800-m isobath (dark gray line) indicates the location of the shelf break and the location of biological hot spots (circles) is shown. Geographic names are abbreviated as LIS—Larsen Ice Shelf, AP—Antarctic Peninsula, GVIIS—George VI Ice Shelf and WIS—Wilkins Ice Shelf.
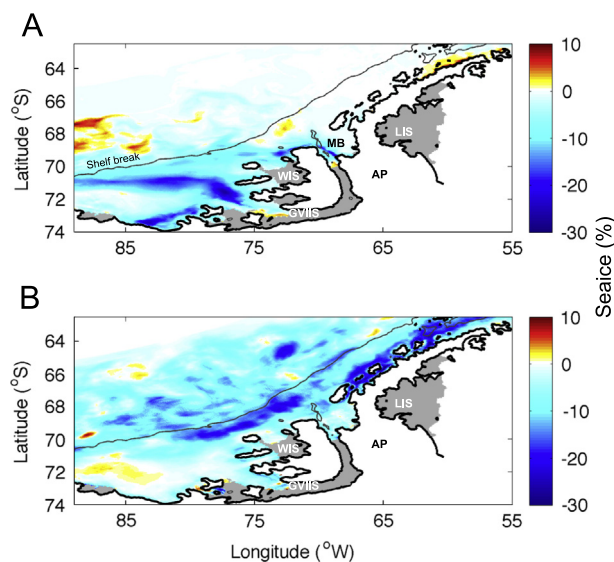
Fig. 10. Percent difference (modified minus present conditions simulations) in the simulated (A) summer and (B) winter sea ice coverage (see Dinniman et al. (2012)). Positive (negative) values indicate more (less) sea ice for increased winds and enhanced ACC transport. The 800-m bathymetric contour (gray line) indicates the shelf break. Geographic names are abbreviated as LIS—Larsen Ice Shelf, AP—Antarctic Peninsula, MB—Marguerite Bay, GVIIS—George VI Ice Shelf and WIS—Wilkins Ice Shelf.
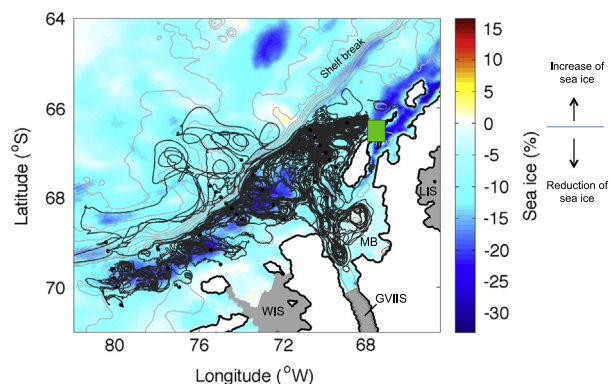
Fig. 11. Simulated particle trajectories (black lines) showing inputs to the biological hot spots regions overlaid on the percent difference (modified minus present conditions simulations) in winter sea ice coverage (same as Fig. 10(B)). Positive (negative) values indicate more (less) sea ice under modified environmental conditions of increased winds and enhanced ACC transport. The Crystal Sound hot spot is shown (green square). The bottom bathymetry (m) from 500 m to 4000 m at 500-m intervals is shown by the light gray lines. Geographic names are abbreviated as LIS—Larsen Ice Shelf, MB—Marguerite Bay, GVIIS—George VI Ice Shelf and WIS—Wilkins Ice Shelf.
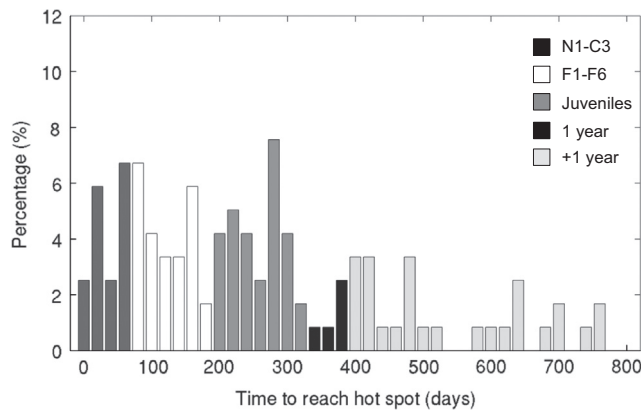
The frequency distribution of the particles reaching the hot spots with times matching the developmental time scales for larvae and 1-year old Antarctic krill, showed that 17.6% of the particles reaching any of the hot spots corresponded to krill larvae from early stages (NI-calyptopis 3) and 25.2% corresponded to larvae in the furcilia stage (Fig. 12). Under projected environmental conditions approximately 42% of inputs to the biological hot spots corresponded to larval stages of Antarctic krill that originated southwest of Marguerite Bay, along the shelf break and the Bellingshausen Sea region.

4. Discussion and summary

4.1. Controls by shelf bathymetry and sea ice

The descent–ascent cycle simulations showed that successful completion of this cycle is possible over most of the wAP shelf;
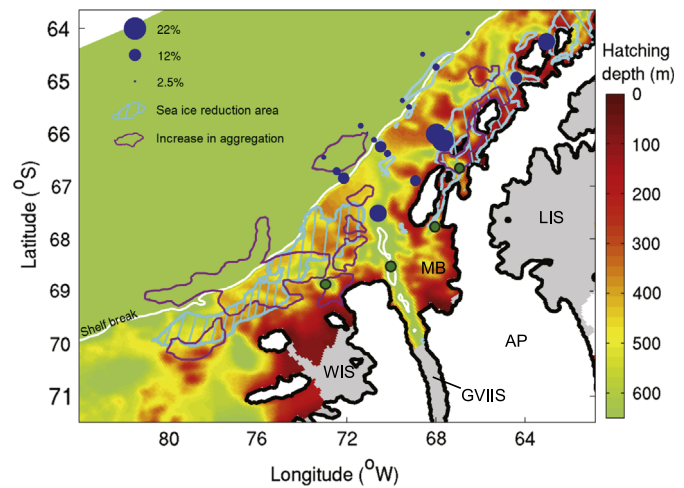
Fig. 12. Frequency distribution of the transport time for the simulated particles that provided inputs to the biological hot spots regions obtained using the modified circulation distributions. The transport times were mapped into Antarctic krill life stages that correspond to nauplius to calyptosis 3 (NI–C3, dark gray bars), furcilia stages (F1–F6, white bars), juveniles (gray bars), 1-year old krill (black bars) and +1 year old krill (light gray bars) using the developmental times given in Table 2.

Fig. 13. Summary of simulated Antarctic krill hatching depths (m, color contours), areas of winter sea ice reduction (blue hatched areas) from simulations that used modified environmental conditions (Dinniman et al. (2012)), increased particle aggregation (purple outline) obtained from Lagrangian simulations using modified conditions, and observations of the percentage of females spawning (Quetin and Ross, 2001; blue dots), an indication of potential spawning regions. The green filled circles indicate the location of the vertical profiles shown in Fig. 5. (For interpretation of the references to color in this figure legend, the reader is referred to the web version of this article.)

a result similar to that obtained using temperature and density climatologies as inputs to the descent–ascent model (Hofmann and Hüsrevoğlu, 2003). However, assuming that the embryo is nonviable or consumed if it hits the bottom prior to hatching limits the areas that support successful completion of the descent–ascent cycle. In most simulations, hatching occurred between 400 and 600 m. Areas of the wAP shelf that are deeper than 500 m are limited to about 30% of the shelf area (Hofmann and Hüsrevoğlu, 2003), implying that only a small portion of this shelf may contribute to successful reproduction of Antarctic krill.

Over most of the wAP continental shelf the descent–ascent cycle takes about 15 days. The presence of modified CDW on the shelf (Klinck et al., 2004; Dinniman and Klinck, 2004) accelerates embryo and larva development (Ross et al., 1988; Hofmann et al., 1992) and assures the successful completion of the cycle in the deeper regions. The shelf region north of Adelaide Island, which supported successful hatching of simulated embryos, is coincident with observed high abundances of Antarctic krill nauplii during the austral summer (Makarov et al., 1990). Eggs were also observed on the shelf, although not in high numbers (50 ind m^{-2}) (Makarov et al., 1990).

Average sea ice duration and extent have been identified as important contributors to krill reproduction and recruitment success (Loeb et al., 1997; Siegel and Loeb, 1995; Ross et al., 1996; Quetin and Ross, 2003; Ducklow et al., 2007). The recruitment index of Antarctic krill is correlated with the timing of sea ice advance, with high recruitment occurring when sea ice advances earlier in the fall (Quetin et al., 1996; Quetin and Ross, 2003) and the duration and extent of winter sea ice affects recruitment success and reproduction (Quetin and Ross, 1991, 2001; Siegel and Loeb, 1995; O'Brien et al., 2011). The simulated winter sea ice distributions obtained from the modified conditions simulations showed a decrease in sea ice in the areas of wAP shelf that are coincident with the biological hot spots and the areas that provide inputs to these regions (Fig. 13). These are also the regions where increased aggregation of particles occurred in response to the modified circulation conditions (Fig. 13). Thus, while the modified circulation conditions may enhance inputs to hot spot regions, the reduced winter sea ice may hinder reproductive output of Antarctic krill and survival of larvae.

In the region north of the Antarctic Peninsula, sea ice coverage is essential to the recruitment success of Antarctic krill (Siegel and Loeb, 1995). For the wAP continental shelf region north of Marguerite Bay, the average pattern in sea ice advance and retreat was found to be positively correlated with good overwinter survival of larvae (Quetin and Ross, 2003) and subsequent recruitment success for Antarctic krill (Ducklow et al., 2007). Observations from the Southern Ocean Global Ocean Ecosystem Dynamics (SO GLOBEC) Program field studies showed that larval krill were primarily in the water column and not necessarily associated with the sea ice habitat of Marguerite Bay (Daly, 2004). Krill reproduction and recruitment in this region were closely related to the spring bloom (Marrari et al., 2008). Sea ice distribution and extent on the wAP sea ice are already changing, with the advance occurring later in the fall and retreat occurring earlier in the spring (Smith and Stammerjohn, 2001; Parkinson, 2002). The modified environmental condition simulations suggest that the Marguerite Bay area will experience similar changes in sea ice timing and extent. Antarctic krill recruitment in the Marguerite Bay region currently does not seem to be directly correlated with sea ice extent and duration as in other areas of the wAP shelf. The projected changes for this region could potentially result in sea ice being more of a factor in Antarctic krill recruitment success, similar to more northern regions.

4.2. Krill reproduction on the shelf

Observations of the abundance and distribution of larval and juvenile Antarctic krill made in the Marguerite Bay region of the wAP shelf during the SO GLOBEC field studies suggested that Antarctic krill reproduction occurs in onshore and offshore areas of the shelf (Ashjian et al., 2004; Daly, 2004; Lawson et al., 2004; Pakhomov et al., 2004; Wiebe et al., 2011). The greatest abundance and biomass of different species of larval krill observed during SO GLOBEC was along the wAP mid shelf to the west of Adelaide Island during fall (Ashjian et al., 2004; Daly, 2004; Pakhomov et al., 2004). This area is coincident with the region that had older stages of krill larvae that originated from simulated particles released in Marguerite Bay southwest of Adelaide Island. These deeper portions of the shelf were also where the descent–ascent cycle was successful.

Additional support for local reproduction of Antarctic krill on the wAP shelf comes from observed zooplankton distribution and abundance patterns (Marrari et al., 2011). Juvenile krill (one year

old) were abundant (132 days m^{-3}) in the fall on the inner shelf around Marguerite Bay, indicating successful recruitment from larvae produced the previous year (Daly, 2004). The depth distribution of Antarctic krill larvae during fall in Laubeuf Fjord (Daly, 2004) showed that late furcilia stages were abundant in the upper 50 m. The Laubeuf Fjord region is a biological hot spot and also one that retained particles for over a year (Piñones et al., 2011, 2013). It is also one of the deeper regions of the inner shelf that supports successful completion of the descent–ascent cycle. Moreover, net samples from the austral fall and winter showed that krill (including Antarctic krill) dominated the zooplankton biomass in the Laubeuf Fjord region between 50 and 100 m (Ashjian et al., 2004; Marrari et al., 2011). This area also showed high backscattering returns (from acoustic surveys), which were related to zooplankton abundance (Lawson et al., 2004; Marrari et al., 2011).

The vertical distribution and abundance of krill larvae obtained from net samples made in fall (Wiebe et al., 2011) showed high abundances of different life stages across the wAP shelf. Off Alexander Island, high abundances of calyptopis (756 days m^{-2}) were observed. This region is also deep which allows completion of the descent–ascent cycle and therefore local reproduction. In this region, the northeasterly flowing shelf currents along the outer part of Alexander Island turn across the wAP shelf along the southern flank of Marguerite Trough north of the hot spot off Alexander Island (Dinniman and Klinck, 2004; Piñones et al., 2011). As a result, the simulated Lagrangian particle trajectories showed that Alexander Island received inputs primarily from the adjacent shelf region from the same area where the highest number of calyptopis were observed.

Video Plankton Recorder measurements made during fall showed that larval euphausiids (includes several species) were present across the entire shelf (Ashjian et al., 2008). Also, high larval abundances were found at depth along a transect that crossed Marguerite Bay, particularly along the portion that crossed Marguerite Trough (Ashjian et al., 2008). Observations from a deep water remotely operated vehicle made during the austral summer showed gravid females above the seabed in Marguerite Trough (Clarke and Tyler, 2008). These adult krill were actively feeding and exoskeletons resulting from molting that may have occurred as the result of spawning were observed. The simulation results indicating that this area of the wAP shelf can support local reproduction and subsequent retention of the early life stages of Antarctic krill are consistent with these observations.

4.3. Implications for lower and higher trophic levels

The habitat of the wAP continental shelf is structured by CDW and sea ice, which in turn have large effects on the ecosystem (Hofmann and Murphy, 2004; Hofmann et al., 2008, 2011; Stammerjohn et al., 2008a; Murphy et al., 2013). Changes in wind speed are already documented for the Southern Ocean (Marshall, 2003; Russell et al., 2006), with strengthening occurring in the Antarctic Peninsula region. Increased winds resulted in increased volume of CDW transported onto the wAP continental shelf and increased vertical mixing of this water into the upper water column (Dinniman et al., 2012). The consequences of this for sea ice were significant, resulting in reductions of summer and winter sea ice extent (Dinniman et al., 2012).

These changes to CDW and sea ice distribution and extent potentially have significant effects on the biological production of wAP region. However, the modified circulation had little effect on the Antarctic krill descent–ascent cycle. Differences in hatching and developmental times between present and modified conditions were small, with the effects confined to limited areas of the shelf. An implication is that successful completion of the descent–ascent cycle on the wAP shelf will not be significantly altered by

the modified environmental conditions. Also, the descent–ascent cycle occurs during summer when little sea ice is present and its effect on this part of the recruitment process is minimal. However, a reduction in winter sea ice has implications for the overwintering success of the larvae resulting from reproduction. This portion of the early life history of Antarctic krill is where the effect of the projected changes to the habitat may potentially have the largest effect.

The simulated mean winter sea ice distribution had the largest reduction (relative to the present conditions simulation) in the mid and inner shelf region of the wAP, which support the biological hot spots as well as successful completion of the descent–ascent cycle. Warming of the shelf waters by greater vertical mixing of CDW may shorten the descent–ascent cycle time due to faster development. However, growth increments and daily growth rates for Antarctic krill across the Scotia Sea decreased with increasing krill length and decreased above a temperature optimum of 0.5°C (Atkinson et al., 2006), suggesting that thermal stress occurs. Increased volume of CDW transported onto the wAP shelf may support faster development of the embryo and larva and contribute to increased reproduction in regions south of Marguerite Bay where depth does not constrain the descent–ascent cycle. Under current conditions, this region has lower temperatures which result in embryos hatching at greater depths. Thus, warming of the wAP shelf south of Marguerite Bay will potentially support embryo hatching and thereby open new areas of the shelf where local krill reproduction can be successful. However, at the same time, warming of the shelf to the north of Marguerite Bay may result in temperatures above 0.5 °C which may affect growth rates. Thus, a consequence of reduced sea ice, increased volume of CDW, and more open water on the wAP shelf may be shifting of the krill habitat boundaries to higher latitudes.

A reduction in sea ice extent and distribution will also affect higher trophic level predators. For example, simulations that linked climate variability and Adélie penguin chick growth and adult foraging showed that environmental changes that reduced prey density or increased adult foraging distance, as will occur with decreased sea ice, had negative impacts on chick success (Chapman et al., 2010). Also, reduced sea ice extent along the wAP may have already limited the distribution of Antarctic silverfish (Fuiman et al., 2002), which is an important prey item for Adélie penguins and their chicks (Chapman et al., 2010). Changes in the habitat are likely to alter the primary production, chlorophyll concentrations, and phytoplankton community composition in wAP shelf waters (Moline and Prézelin, 1996; Montes-Hugo et al., 2009). These changes will affect the quality and quantity of food available to Antarctic krill and also to the higher trophic levels (Ross et al., 2000). Thus, regional warming and associated habitat changes may potentially alter the productivity and structure of the marine food web of the wAP continental shelf.

Acknowledgment

References

Abramowitz, M., Stegun, I.A., 1964. Handbook of Mathematical Functions with Formulas, Graphs, and Mathematical Tables. Tenth Printing AMS IA—National Bureau of Standards Applied Mathematics Series, vol. 55, 1046 pp.
Ashjian, C.J., Rosenwaks, G.A., Wiebe, P.H., Davis, C.S., Gallager, S.M., Copley, N.J., Lawson, G.L., Alatalo, P., 2004. Distribution of zooplankton on the continental

shelf of Marguerite Bay, Antarctic Peninsula, during austral fall and winter, 2001. Deep Sea Research 51, 2073–2098.

Ashjian, C.J., Davis, C.S., Gallager, S.M., Wiebe, P.H., Lawson, G.L., 2008. Distribution of larval krill and zooplankton in association with hydrography in Marguerite Bay, Antarctic Peninsula, in austral fall and winter 2001 described using the Video Plankton Recorder. Deep Sea Research Part II 55, 455–471.

Atkinson, A., Shreeve, R.S., Hirst, A.G., Rothery, P., Tarling, G.A., Pond, D.W., Korb, R. E., Murphy, E.J., Watkins, J.L., 2006. Natural growth rates in Antarctic krill (Euphausia superba): II. Predictive models based on food, temperature, body length, sex, and maturity stage. Limnology and Oceanography 51, 973–987.

Bolmer, S.T., 2008. A note on the development of the bathymetry of the continental margin west of the Antarctic Peninsula from 65° to 71°S and 65° to 78°W. Deep Sea Research Part II 55, 271–276.

Bracegirdle, T.J., Connolley, W.M., Turner, J., 2008. Antarctic climate change over the twenty first century. Journal of Geophysical Research 113, D03103, http://dx. doi.org/10.1029/2007JD008933.

Budgell, W.P., 2005. Numerical simulation of ice–ocean variability in the Barents Sea region. Ocean Dynamics 55, 370–387.

Chapman, E.W., Hofmann, E.E., Patterson, D.L., Fraser, W.R., 2010. The effects of variability in Antarctic krill (Euphausia superba) spawning behavior and sex/ maturity stage distribution on Adélie penguin (Pygoscelis adeliae) chick growth: a modeling study. Deep Sea Research Part II 57, 543–558.

Clarke, A., Tyler, P.A., 2008. Adult Antarctic krill feeding at abyssal depths. Current Biology 18, 282–285.

Costa, D.P., Burns, J.M., Chapman, E., Hildebrand, J., Torres, J.J., Fraser, W., Fried-lander, A., Ribic, C., Halpin, P., 2007. US SO GLOBEC Predator Programme. GLOBEC International Newsletter 13, 62–66.

Daly, K.L., 1990. Overwintering development, growth, and feeding of larval Euphausia superba in the Antarctic marginal ice zone. Limnology and Oceano-graphy 35 (7), 1564–1576.

Daly, K.L., 2004. Overwintering growth and development of larval Euphausia superba: an interannual comparison under varying environmental conditions west of the Antarctic Peninsula. Deep Sea Research Part II 51, 2139–2168.

Dinniman, M.S., Klinck, J.M., 2004. A model study of circulation and cross-shelf exchange on the west Antarctic Peninsula continental shelf. Deep Sea Research Part II 51, 2003–2022.

Dinniman, M.S., Klinck, J.M., Smith, W.O., 2007. Influence of sea ice cover and icebergs on circulation and water mass formation in a numerical circulation model of the Ross Sea, Antarctica. Journal of Geophysical Research 112 (C11013), 1–13.

Dinniman, M.S., Klinck, J.M., Smith, W.O., 2011. A model study of circumpolar deep water on the west Antarctic Peninsula and Ross Sea continental shelves. Deep Sea Research Part II 58, 1508–1523.

Dinniman, M.S., Klinck, J.M., Hofmann, E.E., 2012. Sensitivity of circumpolar deep water transport and ice shelf basal melt along the west Antarctic Peninsula to changes in the winds. Journal of Climate 25, 4799–4816.

Ducklow, H.W., Baker, K., Martinson, D.G., Quetin, L.B., Ross, R.M., Smith, R.C., Stammerjohn, S.E., Vernet, M., Fraser, W., 2007. Marine pelagic ecosystems: the west Antarctic Peninsula. Philosophical Transactions of the Royal Society B 362, 67–94.

Fraser, W.R., Hofmann, E.E., 2003. A predators perspective on causal links between climate change, physical forcing and ecosystem response. Marine Ecology Progress Series 265, 1–15.

Fuiman, L.A., Davis, R.W., Williams, T.M., 2002. Behavior of midwater fishes under the Antarctic ice: observations by a predator. Marine Biology 140, 815–822.

Haidvogel, D.B., Arango, H., Budgell, W., Cornuelle, B., Curchitser, E., Dilorenzo, E., Fennel, K., Geyer, W., Hermann, A., Lanerolle, L., 2008. Ocean forecasting in terrain-following coordinates: formulation and skill assessment of the Regio-nal Ocean Modeling System. Journal of Computational Physics 227, 3595–3624, http://dx.doi.org/10.1016/j.jcp.2007.06.016.

Hamming, R.W, 1973. Numerical Methods for Scientists and Engineers, 2nd ed. McGraw-Hill, New York p. 721.

Hempel, I., Hempel, G., 1986. Field observations on the developmental ascent of larval Euphausia superba (Crustacea). Polar Biology 6, 121–126.

Hofmann, E.E., Hüsrevoğlu, Y.S., 2003. A circumpolar modeling study of habitat control of Antarctic krill (Euphausia superba) reproductive success. Deep Sea Research Part II 50, 3121–3142.

Hofmann, E.E., Murphy, E.J., 2004. Advection, krill, and Antarctic marine ecosys-tems. Antarctic Science 16, 487–499.

Hofmann, E.E., Capella, J.E., Ross, R.M., Quetin, L.B., 1992. Models of the early life history of Euphausia superba—Part I. Time and temperature dependence during the descent–ascent cycle. Deep Sea Research Part I 39 (7–8), 1177–1200.

Hofmann, E.E., Lascara, C.M., 2000. Modeling the growth dynamics of Antarctic krill (Euphausia superba). Marine Ecology Progress Series 194, 219–231.

Hofmann, E.E., Wiebe, P.H., Costa, D.P., Torres, J.J., 2008. Introduction to dynamics of plankton, krill, and predators in relation to environmental features of the western Antarctic Peninsula and related areas: SO GLOBEC Part II. Deep Sea Research Part II 55, 269–270.

Hofmann, E.E., Wiebe, P.H., Costa, D.P., Torres, J.J., 2011. Introduction to under-standing the linkages between Antarctic food webs and the environment: a synthesis of Southern Ocean GLOBEC studies. Deep Sea Research Part II 58, 1505–1507.

Hunter, J.R., Craig, P.D., Phillips, H.E., 1993. On the use of random walk models with spatially variable diffusivity. Journal of Computational Physics 106 (2), 366–376.

Ikeda, T., 1984. Development of the larvae of the Antarctic krill (Euphausia superba Dana) observed in the laboratory. Journal of Experimental Marine Biology and Ecology 75, 107–117.

Kanda, K., Takagi, K., Seki, Y., 1982. Movement of the larger swarms of Antarctic krill Euphausia superba population off Enderby Land during 1976–1977 season. Journal of the Tokyo University of Fisheries 68, 25–42.

Klinck, J.M., 1998. Heat and salt changes on the continental shelf west of the Antarctic Peninsula between January 1993 and January 1994. Journal of Geophysical Research 103, 7617–7636.

Klinck, J.M., Hofmann, E.E., Beardsley, R.C., Salihoğlu, B., Howard, S., 2004. Water-mass properties and circulation on the west Antarctic Peninsula Continental Shelf in Austral Fall and Winter 2001. Deep Sea Research Part II 51, 1925–1946.

Lascara, C.M., Hofmann, E.E., Ross, R.R., Quetin, L.B., 1999. Seasonal variability in the distribution of Antarctic krill, Euphausia superba, west of the Antarctic Penin-sula. Deep Sea Research Part I 46, 925–949.

Lawson, G.L., Wiebe, P.H., Ashjian, C.J., Gallager, S.M., Davis, C.S., Warren, J.D., 2004. Acoustically inferred zooplankton distribution in relation to hydrography west of the Antarctic Peninsula. Deep Sea Research Part II 51, 2041–2072.

Lawson, G.L., Wiebe, P.H., Ashjian, C.J., Stanton, T.K., 2008. Euphausiid distribution along the western Antarctic Peninsula—Part B: distribution of euphausiid aggregations and biomass, and associations with environmental features. Deep Sea Research Part II 55, 432–454.

Lubin, D., Wittenmyer, R.A., Bromwich, D.H., Marshall, G.J., 2008. Antarctic Peninsula mesoscale cyclone variability and climate impacts influenced by the SAM. Geophysical Research Letters 35, L02808, http://dx.doi.org/10.1029/2007GL032170.

Liu, J., Curry, J.A., Martinson, D.G., 2004. Interpretation of recent Antarctic sea ice variability. Geophysical Research Letters 31, L02205, http://dx.doi.org/10.1029/2003GL018732.

Loeb, V., Siegel, V., Holm-Hansen, O., Hewitt, R.P., Fraser, W., Trivelpiece, W.Z., Trivelpiece, S., 1997. Effects of sea-ice extent and krill or salp dominance on the Antarctic food web. Nature 387 (6636), 897–900.

Makarov, R., Enshenina, L.M., Spiridonov, V., 1990. Distributional ecology of euphausiid larvae in the Antarctic Peninsula region and adjacent waters. Proceedings of the NIPR Symposium on Polar Biology 3, 23–35.

Marshall, G.J., 2003. Trends in the Southern Annular Mode from observations and reanalyses. Journal of Climate 16, 4134–4143.

Marshall, G.J., Orr, A., van Lipzig, N.P.M., King, J.C., 2006. The impact of a changing Southern Hemisphere Annular Mode on Antarctic Peninsula summer tempera-tures. Journal of Climate 19, 5388–5404.

Marr, J.W.S., 1962. The natural history and geography of the Antarctic krill Euphausia superba Dana. Discovery Report 32, 37–465.

Marrari, M., Daly, K.L., Hu, C., 2008. Spatial and temporal variability of SeaWiFS derived chlorophyll distributions west of the Antarctic Peninsula: implications for krill production. Deep Sea Research Part II 55, 377–392.

Marrari, M., Daly, K.L., Timonin, A., Semenova, T., 2011. The zooplankton of Marguerite Bay, Western Antarctic Peninsula. Part I: abundance, distribution, and population response to variability in environmental conditions. Deep Sea Research Part II 58, 1599–1613.

Meredith, M.P., King, J.C., 2005. Rapid climate change in the ocean west of the Antarctic Peninsula during the second half of the 20th century. Geophysical Research Letters 32, L19604.

Milliff, R.F., Morzel, J., Chelton, D.B., Freilich, M.H., 2004. Wind stress curl and wind stress divergence biases from rain effects on QSCAT surface wind retrievals. Journal of Atmospheric and Oceanic Technology 21, 1216–1231.

Moffat, C., Owens, B., Beardsley, R.C., 2009. On the characteristics of Circumpolar Deep Water Intrusions to the west Antarctic Peninsula Continental Shelf. Journal of Geophysical Research 114, C05017, http://dx.doi.org/10.1029/2008JC004955.

Moline, M.A., Prézelin, B.B., 1996. Long-term monitoring and analyses of physical factors regulating variability in coastal Antarctic phytoplankton biomass, in situ productivity and taxonomic composition over subseasonal, seasonal and interannual time scales. Marine Ecology Progress Series 145, 143–160.

Montes-Hugo, M., Doney, S.C., Ducklow, H.W., Fraser, W., Martinson, D., Stammer-john, S.E., Schofield, O., 2009. Recent changes in phytoplankton communities associated with rapid regional climate change along the western Antarctic Peninsula. Science 323, 1470–1473.

Murphy, E.J., Hofmann, E.E., Watkins, J.L., Johnston, N.M., Piñones, A., Ballerini, T., Hill, S.L., Trathan, P.N., Tarling, G.A., Cavanagh, R.A., Young, E.F., Thorpe, S., Fretwell, P., 2013. Comparison of the structure and function of Southern Ocean regional ecosystems: the Antarctic Peninsula and South Georgia. Journal of Marine Systems 109–110, 22–42.

Nicol, S., 2003. Krill and currents—physical and biological interactions influencing the distribution of Euphausia superba. Ocean and Polar Research 24 (4), 633–644.

O'Brien, C., Virtue, P., Kawaguchi, S., Nichols, P.D., 2011. Aspects of krill growth and condition during late winter-early spring off East Antarctica (110–130°E). Deep Sea Research Part II 58, 1211–1221.

Pakhomov, E.A., Atkinson, A., Meyer, B., Oettl, B., Bathmann, U., 2004. Daily ratios and growth of larval Antarctic krill Euphausia superba in the Eastern Bellingshausen Sea during austral autumn. Deep Sea Research Part II 51, 2185–2198.

Parkinson, C.L., 2002. Trends in the length of the Southern Ocean sea ice season, 1979–1999. Annals of Glaciology 34, 435–440.

Piñones, A., Hofmann, E.E., Dinniman, M.S., Klinck, J.M., 2011. Lagrangian simulation of transport pathways and residence times along the western Antarctic Peninsula. Deep Sea Research Part II 58, 1524–1539.

Piñones, A., Hofmann, E.E., Daly, K.L., Dinniman, M.S., Klinck, J.M., 2013. Modeling the remote and local connectivity of Antarctic krill populations along the western Antarctic Peninsula. Marine Ecology Progress Series 481, 69–92.

Quetin, L.B., Ross, R.M., 1984. Depth distribution of developing *Euphausia superba* embryos, predicted from sinking rates. Marine Biology 79, 47–53.

Quetin, L.B., Ross, R.M., 1989. Effects of oxygen, temperature and age on the metabolic rate of the embryos and early larval stages of the Antarctic krill *Euphausia superba* Dana. Journal of Experimental Marine Biology and Ecology 125, 43–62.

Quetin, L.B., Ross, R.M., 1991. Behavioral and physiological characteristics of the Antarctic krill *Euphausia superba*. American Zoologist 31, 49–63.

Quetin, L.B., Ross, R.M., 2001. Environmental variability and its impact on the reproductive cycle of Antarctic krill. American Zoologist 41, 74–89.

Quetin, L.B., Ross, R.M., 2003. Episodic recruitment in Antarctic krill *Euphausia superba* in the Palmer LTER study region. Marine Ecology Progress Series 259, 185–200.

Quetin, L.B., Ross, R.M., Frazer, T.K., Haberman, K.L., 1996. Factors affecting distribution and abundance of zooplankton, with an emphasis on Antarctic krill, *Euphausia superba*. In: Ross, R.M., Hofmann, E.E., Quetin, L.B. (Eds.), Foundations for Ecological Research West of the Antarctic Peninsula, vol. 70. American Geophysical Union, Washington, DC, pp. 357–371.

Ross, R.M., Quetin, L.B., 1986. How productive are Antarctic krill? Bioscience 36, 264–269.

Ross, R.M., Quetin, L.B., 1989. Energetic cost to develop to the first feeding stage of *Euphausia superba* Dana and the effect of delays in food availability. Journal of Experimental Marine Biology and Ecology 133, 103–127.

Ross, R.M., Quetin, L.B., Kirsch, E., 1988. Effect of temperature on developmental times and survival of early larval stages of *Euphausia superba* Dana. Journal of Experimental Marine Biology and Ecology 121, 55–71.

Ross, R.M., Quetin, L.B., Lascara, C.M., 1996. Distribution of Antarctic krill and dominant zooplankton west of the Antarctic Peninsula. In: Ross, R.M., Hofmann, E.E., Quetin, L.B. (Eds.), Foundations for Ecological Research West of the Antarctic Peninsula. AGU Antarctic Research Series. America Geophysical Union, Washington, DC, pp. 199–217.

Ross, R.M., Quetin, L.B., Baker, K.S., Vernet, M., Smith, R.C., 2000. Growth limitation in young *Euphausia superba* under field conditions. Limnology and Oceanography 45, 31–43.

Ross, R.M., Quetin, L.B., Martinson, D.G., Iannuzzi, R.A., Stammerjohn, S.E., Smith, R.C., 2008. Palmer LTER: patterns of distribution of five dominant zooplankton species in the epipelagic zone west of the Antarctic Peninsula, 1993–2004. Deep Sea Research Part II 55, 2086–2105.

Russell, J.L., Dixon, K.W., Gnanadesikan, A., Stouffer, R.J., Toggweiler, J.R., 2006. The Southern Hemisphere westerlies in a warming world: propping open the door to the deep ocean. Journal of Climate 19, 6382–6390.

Savidge, D.K., Amft, J.A., 2009. Circulation on the West Antarctic Peninsula derived from 6 years of shipboard ADCP transects. Deep Sea Research Part I 56, 1633–1655.

Shchepetkin, A.F., McWilliams, J.C., 2009. Correction and commentary for "Ocean forecasting in terrain-following co-ordinate: formulation and skill assessment of the regional ocean modeling system" by Haidvogel et al., J. Comp. Phys. 227, pp. 3595–3634. Journal of Computational Physics 228, 8985–9000, http://dx.doi.org/10.1016/ j.jcp.2009.09.002.

Siegel, V., 1988. A concept of seasonal variation of krill (*Euphausia superba*) distribution and abundance west of the Antarctic Peninsula. In: El-Sayed, S.Z. (Ed.), Antarctic Ocean and Resources Variability. Springer-Verlag, Berlin Heidelberg, Paris, pp. 219–230.

Siegel, V., 1992. Assessment of the krill (*Euphausia superba*) spawning stock off the Antarctic Peninsula. Archiv fur Fischereiwissenschaft 41, 101–130.

Siegel, V., 2000a. Krill (Euphausiacea) life history and aspects of population dynamics. Canadian Journal of Fisheries and Aquatic Sciences 57, 130–150.

Siegel, V., 2000b. Krill demography and variability in abundance and distribution. Canadian Journal of Fisheries and Aquatic Sciences 57, 151–167.

Siegel, V., Loeb, V., 1995. Recruitment of Antarctic krill *Euphausia superba* and possible causes for its variability. Marine Ecology Progress Series 123, 45–56.

Smith, R.C., Stammerjohn, S.E., 2001. Variations of surface air temperature and sea-ice extent in the western Antarctic Peninsula region. Annals of Glaciology 33, 493–500.

Spiridonov, V.A., 1995. Spatial and temporal variability in reproductive timing of Antarctic krill (*Euphausia superba* dana). Polar Biology 15, 161–174.

Stammerjohn, S.E., Martinson, D.G., Smith, R.C., Iannuzzi, R.A., 2008a. Sea ice in the western Antarctic Peninsula region: spatio-temporal variability from ecological and climate change perspectives. Deep Sea Research Part II 55, 2041–2058.

Stammerjohn, S.E., Martinson, D.G., Smith, R.C., Yuan, X., Rind, D., 2008b. Trends in Antarctic annual sea ice retreat and advance and their relation to El Niño–Southern Oscillation and Southern Annular Mode variability. Journal of Geophysical Research 113, C03S90, http://dx.doi.org/10.1029/2007JC004269.

Thompson, D.W.J, Wallace, J.M., Hegerl, G.C., 2000. Annular modes in the extratropical circulation. Part II: Trends. Journal of Climate 13, 1018–1036.

Thompson, D.W.J, Solomon, S., 2002. Interpretation of recent Southern Hemisphere climate change. Science 296, 895–899.

Vaughan, D.G., Marshall, G.J., Connolley, W.M., Parkinson, C., Mulvaney, R., Hodgson, D.A., King, J.C., Pudsey, C.J., Turner, J., 2003. Recent rapid regional climate warming on the Antarctic Peninsula. Climatic Change 60, 243–274.

Visser, A.W., 1997. Using random walk models to simulate the vertical distribution of particles in a turbulent water column. Marine Ecology Progress Series 158, 275–281.

Wiebe, P.H., Ashjian, C.J., Lawson, G.L., Piñones, A., Copley, N.J., 2011. Horizontal and vertical distribution of euphausiid species on the Western Antarctic Peninsula US GLOBEC Southern Ocean study site. Deep Sea Research Part II 58, 1630–1651.

Witek, Z., Koronkiewicz, A., Soszka, G.J., 1980. Certain aspects of the early life history of krill *Euphausia superba* Dana (crustacea). Polish Polar Research 1, 97–115.